ELSEVIER

Journal of Organometallic Chemistry 571 (1998) 43–53

Journal of Organometallic Chemistry

Substituted cyclopentadienyl compounds. Part V. NMR and extended Hückel studies of the isomeric preferences of some main group metal cyclopentadienide compounds and a reinvestigation of the crystal structure of thallium(I) tricyanovinylcyclopentadienide[1]

Michael Arthurs [a,*], John C. Bickerton [a], Graeme Hogarth [b], D. Antony Morton-Blake [c], Gina Kubal [a], Mary R. Truter [b]

[a] *Division of Chemistry and Environmental Sciences, Coventry University, Priory Street, Coventry CV1 5FB, UK*
[b] *Chemistry Department, University College London, 20 Gordon Street, London WC1H 0AJ, UK*
[c] *Chemistry Department, University of Dublin, Trinity College, Dublin 2, Ireland*

Received 27 April 1998

Abstract

Solution NMR studies have been performed on a series of mono-substituted cyclopentadienide salts, $[M^+(C_5H_4X^-)]$ (M = Li, Na, K, Cs, Tl; X = $CONMe_2$, COOMe, COC_6H_5, COMe, CHO, $COCO_2C_2H_5$, NO_2 and $C(CN)=C(CN)_2$). Population of a fulvenoid isomer in which the dominant bonding mode involves interaction between the cation and the ring substituent heteroatom is enhanced when X is strongly electron accepting and the cation is a hard Lewis acid. An alternate isomer involving a bonding interaction between the cyclopentadienyl carbon atoms and the metal ion predominates when X is weakly accepting and the cation is a soft Lewis acid. A range of compounds between these two isomeric extremes show fluxional behaviour in dimethyl sulphoxide (DMSO) solvent. Within the series of alkali metal salts and for a given X group, the maximum barrier for interconversion of isomers is achieved when M is potassium. This phenomenon is attributed to the balance between Lewis character and solvation of the cation in DMSO. Molecular orbital calculations based on the extended Hückel method were performed to examine the effect of the chemical nature of X and M on the relative energies of the isomers. These suggest that the energy separation is more sensitive to the nature of X than of M, but that the electronegativity of M also plays a role by its effect in shifting the energies into critical π-MO energy ranges. The single crystal X-ray structure of a representative derivative, $Tl[C_5H_4C(CN)=C(CN)_2]$ has been reinvestigated. It shows a complex 3D structure in which each thallium is bonded to four nitrogen atoms and a single cyclopentadienide ring, a situation entirely consistent with the behaviour of this compound in solution in which the fulvenoid isomer is dominant.

Keywords: Cyclopentadienides; Fluxionality; Crystal structure; Extended Hückel calculations; Nuclear magnetic resonance

1. Introduction

The origins of this work stem from the research of Thiele [2] and more recent studies by Hafner et al. [3] on alkali metal salts of mono-substituted cyclopentadienes. There has been extensive investigation into the nature of species present in solutions of cyclopentadienide [4,5], indenide [6] and fluorenide [7] salts of the alkali metals. In contrast, the sole, systematic study of salts of cyclopentadiene in which the ring carries one electron-accepting group involved the NMR study of lithium derivatives of acetyl, methoxycarbonyl and *t*-butylformylcyclopentadiene in tetrahydrofuran (THF) and hexamethylphosphoric triamide solvents (HMPA)

* Corresponding author. Fax: +01 203 838793; e-mail: apx052@cov.ac.uk

[1] For part IV, see Hogarth et al. [1].

0022-328X/98/$ - see front matter
PII S0022-328X(98)00849-3

[8]. These salt solutions comprise solvent-separated ion pairs in which the species present exist mainly as a population distribution of fulvenoid (**A**) and cyclopentadienide (**B**) isomers.

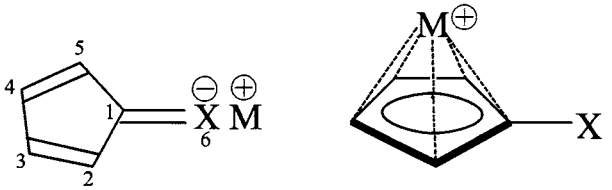

(A) **(B)**

In this paper we extend this study to include lithium, sodium, potassium, caesium and thallium(I) salts of a series of mono-substituted cyclopentadienes in which the ring substituent ranges from the weakly accepting $-CONMe_2$ to the very strongly accepting $-C(CN)=C(CN)_2$ group. The dominant role of the substituent is electronic rather than steric in each case. Solution NMR studies supported by extended Hückel molecular orbital calculations permit a detailed analysis of the factors which govern the structural trends in the series.

2. Experimental

All solvents were distilled prior to use and stored over appropriate drying agents. Synthetic operations were effected under an atmosphere of argon. ^{1}H- and ^{13}C-NMR solution spectra were recorded on Bruker AC-250, WH-400 and WM-500 spectrometers fitted with variable temperature accessories. The probe temperature was calibrated with methanol below ambient temperature and with 1,2-dihydroxyethane above it [9]. Free energies of activation were calculated from ^{13}C-NMR data using Eq. (1) [10]:

$$\Delta G^{\#} = -RT_c \ln \frac{\pi \Delta v h}{\sqrt{2}\, kT_c} \quad (1)$$

where Δv is the chemical shift difference between the coalescing resonances in the absence of exchange, T_c is the coalescence temperature (K) and R, h and k have their usual thermodynamic significance. An approximate value of $\Delta G^{\#}$ was determined from the ^{1}H-NMR spectrum of **28** by line shape analysis of the AA′XX′ pattern [11] using methods analogous to those of Roberts [12]. The solid-state ^{13}C-NMR spectrum of **31** was recorded at 75.5 MHz (7.05 T) on a Bruker MSL300 spectrometer using a standard Bruker magic angle sample (MAS) probe with double-bearing rotation mechanism. The sample was studied as a polycrystalline powder in zirconia rotors (7 mm external diameter and a MAS frequency of 4.07 kHz with a stability better than ± 10 Hz). The pulse sequences for total suppression of spinning sidebands (TOSS) [13,14] and for the combination of TOSS with dipolar dephasing (non-quaternary suppression, NQS) [15] were used. The spectra were recorded at ambient probe temperature with chemical shifts relative to TMS.

Compounds **4** [16], **5** [8], **9** [17], **11** [18], **14** [18], **15** [8], **17** [19], **19** [19], **22** [20], **24** [19], **25** [2], **26** [20], **27** [21], **28** [20] and **31** [22], were prepared and analysed by published procedures. The remaining alkali metal compounds were synthesised by metathesis reactions involving the appropriate thallium cyclopentadienide precursor with the metal iodide in $(CD_3)_2SO$ solvent. In a typical preparation, equimolar $(CD_3)_2SO$ solutions of CsI (520 mg, 2.0 cm^3) and $TlC_5H_4-C(CN)=C(CN)_2$ (742 mg, 2.0 cm^3) were mixed under argon. The reaction was instantaneous and quantitative. After filtering off the bright yellow precipitate of thallium iodide, the residual solution was promptly analysed by NMR spectroscopy. The salt solutions in $(CD_3)_2SO$ showed ^{1}H- and ^{13}C-NMR spectra independent of the method of preparation. The concentration of the analyte solutions varied from 0.25 to 0.50 M depending upon the solubility of the thallium precursor. Variable temperature NMR studies were carried out over the temperature range 20–100°C and chemical shifts are relative to TMS.

3. X-ray analysis of 31

Dark red air-stable plates were obtained by slow recrystallisation from acetonitrile at 10°C. A suitable crystal of approximate size $0.30 \times 0.20 \times 0.08$ mm was mounted on a glass fibre.

3.1. Crystal data

$C_{10}H_4N_3Tl$, $M = 370.53$, monoclinic, $a = 7.904(2)$, $b = 10.004(2)$, $c = 13.079(3)$ Å, $\beta = 111.45(3)°$, $U = 962.54(4)$ Å^3 (by least-squares refinement on diffractometer angles for 28 automatically centred ($16 \leq 2\theta \leq 30°$) reflections, $\lambda = 0.71073$ Å, space group $P2_1/c$, $Z = 4$, $D_{calc.} = 2.557$ g cm^{-3}, $F(000) = 664$, μ(Mo–K$_\alpha$) = 167.37 cm^{-1}.

3.2. Data collection and processing

Nicolet R3 mV diffractometer, $T = 19°C$, ω-2θ mode, graphite monochromated Mo–K$_\alpha$ radiation; 1787 reflections measured ($5 \leq 2\theta \leq 50°$, h, k, $\pm l$), 1669 unique. Three standard reflections (remeasured every 97 scans) showed no significant loss of intensity during data collection; 1664 reflections with $I > 2\sigma(I)$. Data corrected for Lorentz and polarisation effects and empirically for absorption; (max. 1.000, min. 0.413).

3.3. Structure analysis and refinement

Initial structure solution was by direct methods being developed using alternating cycles of least-squares refinement and difference Fourier synthesis. Non-hydrogen atoms were refined anisotropically and hydrogens in calculated positions (C–H = 0.96 Å) with one, overall refined isotropic thermal parameter ($U_{iso} = 0.08$ Å^2).

The weighting scheme $w = 1/[\sigma^2(F_o) + 0.000465\ F_o^2]$ gave satisfactory agreement analyses. The final cycle of least-squares refinement included 127 parameters for 1664 variables and did not shift any parameter by more than 0.001 times its' S.D. Final R and R_w values were 0.0417 and 0.1068, respectively. The final difference-Fourier showed one peak of 1.04 e Å^{-3}, close to the thallium atom. Solution of the structure employed the SHELXTL PLUS program package on a MicroVAX II computer. Atomic co-ordinates are given in Table 2 and bond angles and distances in Table 3. Tables of equivalent isotropic and anisotropic displacement parameters, H atom co-ordinates, bond lengths, bond angles and structure factors have been deposited at the Cambridge Crystallographic Data Centre.

4. Results and discussion

4.1. NMR spectra

The objective of the NMR study was to establish the relative importance of isomers (**A**) and (**B**) in $(CD_3)_2SO$ solution over the temperature range 20–100°C. Because of the low solubility of the thallium derivatives in most common solvents and the need to avoid hydroxylic solvents which facilitate H–D exchange with the Cp ring hydrogens [23], dimethylsulphoxide was the solvent of choice. Table 1 gives the ^{13}C-NMR data at 25°C along with some estimated free energies of activation ($\Delta G^{\#}$) for rotation about the C(1)–X bond.

Structure (**A**) has a planar fulvenoid conformation by which the excess electron of the Cp system is distributed over the substituent. There is also an appreciable barrier to rotation about the C(1)–X bond. In the case of isomer (**B**) there is free rotation about this bond. For a given carbanion of the type shown in Table 1, the formation of solvent-separated ion pairs is facilitated by use of: (a) a small metal cation; (b) a decrease in solution temperature; and (c) a powerful solvating solvent (such as dimethylsulphoxide). Assuming that all the compounds in Table 1 are present as solvent-separated ion pairs, the perturbation of the carbanion electron shell resulting from the proximity of the cation should be relatively small [24] and consequently there should be minimal differences in the ^{13}C-NMR spectrum of a given $[C_5H_4X]^-$ system with variation in the metal ion. Compounds **1**–**31** show one of two types of ^{13}C-NMR spectra for the Cp ring carbons. In the case of compounds **1**–**9**, **14**, **19**, and **24**, a low intensity peak is assigned to the nodal carbon, C(1) and the atom pairs, C(2), C(5) and C(3), C(4) each give a single peak. These spectra are temperature independent. The corresponding ^{1}H-NMR spectra give two pseudo-triplets characteristic of an AA′XX′ system in which $^3J_{AX}$ and $^4J_{AX'}$ are of similar magnitude. This pseudo-A_2X_2 pattern is associated with Cp systems in which there is rapid rotation about C(1)–C(6). The chemical shift of C(6), the carbon attached to the substituent heteroatom, is a sensitive indicator of the isomer present in solution [25]. Thus, in compounds **1**–**9** there is little variation in this chemical shift and a spectral pattern consistent with population of structure (**B**) in solution. A similar pattern is noted for compounds **27** and **28**. However, in this case the ^{1}H-NMR spectra show all the characteristics of an AA′XX′ pattern consistent with population of structure (**A**) in which there is a high barrier to free rotation about the C–NO_2 bond [20]. This spectral pattern was also noted for K(C_5H_4CN) [26] and is again associated with the symmetry of the substituent and the hindered rotation about the C(1)–X bond. In the case of **27** and **28** the strongly accepting –NO_2 group tends to localise charge density on the oxygen atoms of the heteroatom and Table 1 shows that the barrier to rotation about C(1)–X is lower in the case of the thallium(I) compound.

The second ^{13}C spectral type associated with an ADMX pattern is shown by the remaining compounds in Table 1. In the case of **29**–**31** where the substituent is the most electron-accepting of the series, each ring carbon shows a sharp singlet and the spectra are temperature independent between 20–100°C. This is associated with population of an isomer in which there is no free rotation about C(1)–C(6), and again there is little variation in the heteroatom (cyanide) carbons from lithium to thallium. The olefinic carbon atoms of the tricyanovinyl group show two resonances (δ: 123.60 =*C*(CN) and 119.20 ppm =*C*$(CN)_2$). These equate with small deshielding contributions of 11.1 and 6.7 ppm, respectively, relative to tetracyanoethene [27]. Compounds in which the tricyanoyinyl group is covalently bonded to a transition metal, e.g. [$(NC)_2$C=C(CN)W-$(CO_3Cp]$ show a large downfield shift (50–60 ppm) for the olefinic carbon atom to which the metal is bonded and a small upfield shift (ca. 6 ppm) for the terminal olefinic carbon. In addition it is noteworthy that the tungsten compound shows a separate resonance for each cyano group (δ: =C(*C*N) 120.60, =C$(CN)_2$ 112.70 and 114.90 ppm) while compounds **29**–**31** give only a broad resonance centred at 112.40 ppm for the cyano groups at ambient temperature. On warming a $(CD_3)_2SO$ solution of **31** to 60°C, this signal now gives a sharp peak. The X-ray crystal structure of **31** shows that each –CN group is bonded to a thallium

Table 1
^{13}C-NMR data[a] for M(C_5H_4X) compounds in $(CD_3)_2SO$ at 298 K with isomer preferences[b] and $\Delta G^{\#}$ values[c] for rotation about C(1)–C(6)

M	X	$CONMe_2$		COOMe		COC_6H_5		COMe		CHO		$COCO_2Et$		NO_2		$C(CN)=C(CN)_2$
Li	**1**	(170.14)	**5**	(167.60)	**10**	(185.33)	**15**	(187.05)	**20**	(179.37)					**29**	(122.40)
		118.12		113.09		123.99		126.18		126.76						131.50
		113.22		113.37		116.85		114.01		110.59						116.32
		109.69		111.44		114.76		113.41		117.03						124.55
										114.00						122.59
										120.64						129.23
		[**B**]		[**B**]		[50.5]		[54.5]		[58.4]						[**A**]
Na	**2**	(170.69)	**6**	(167.56)	**11**	(185.85)	**16**	(189.84)	**21**	(180.94)	**25**	(174.69)	**27**			
		118.15		112.72		123.77		125.95		127.06		(170.57)				
		113.17		113.32		116.28		113.79		115.51		120.70		134.97		
		109.68		111.58		114.27		113.23		(Broad)		113.30		116.62		
												114.89		112.08		
												117.22				
												118.52				
		[**B**]		[**B**]		[**B**]		[53.0]		[54.5]		[**A**]		[**A**]		
K			**7**	(167.79)	**12**	(187.18)	**17**	(187.40)	**22**	(180.20)						
				112.65		124.01		125.08		126.55						
				113.48		116.04		115.81		109.63						
				111.78		114.17		113.98		116.40						
								112.14		113.48						
										119.89						
				[**B**]		[51.5]		[61.4]		[67.1]						
Cs	**3**	(170.11)	**8**	(167.55)	**13**	(186.17)	**18**	(190.17)	**23**	(180.13)					**30**	(122.53)
		118.18		112.74		123.83		126.61		126.75						131.43
		113.12		113.33		116.19		114.26		110.05						116.25
		109.60		111.59		114.13		113.12		116.50						124.51
										113.55						122.71
										120.04						129.18
		[**B**]		[**B**]		[50.0]		[53.8]		[57.3]						[**A**]
Tl	**4**	(170.45)	**9**	(168.51)	**14**	(189.17)	**19**	(191.57)	**24**	(183.50)	**26**	(178.14)	**28**		**31**	(122.35)
		118.50		113.59		124.65		126.61		127.67		(169.09)				131.42
		113.38		113.47		116.03		113.63		116.10		121.20		135.57		116.30
		109.82		111.79		114.13		113.25		114.99		116.83		116.35		124.60
												115.56		111.89		123.46
																129.26
		[**B**]		[**B**]		[**B**]		[**B**]		[**B**]		[57.4]		[90.0]		[**A**]

[a] Chemical shifts are listed in the sequence: C(X) (in parentheses), C(1), C(2), C(3), C(4) and C(5) relative to internal TMS.
[b] Principal isomer present **A** or **B** (in square brackets).
[c] $\Delta G^{\#} \pm 2.0$ kJ mol^{-1} (in square brackets).

Table 2
Atomic coordinates ($\times 10^4$) and equivalent isotropic displacement parameters (Å $\times 10^3$) for Tl[$C_5H_4C(CN)=C(CN)_2$]

Atom	x	y	z	U^a_{eq}
Tl	8939(1)	1220(1)	3391(1)	53(1)
N(1)	5357(17)	5710(14)	2949(10)	73(3)
N(2)	6679(19)	2319(14)	−383(11)	76(3)
N(3)	2291(17)	4024(13)	288(9)	67(3)
C(1)	8807(15)	4035(12)	2390(9)	45(3)
C(2)	10104(17)	3287(12)	2053(10)	52(3)
C(3)	11764(17)	3391(13)	2878(12)	58(3)
C(4)	11619(18)	4172(14)	3768(10)	60(3)
C(5)	9825(18)	4539(12)	3468(10)	52(3)
C(6)	6908(20)	4184(13)	1910(11)	56(3)
C(7)	5712(16)	3670(13)	929(10)	55(3)
C(8)	5959(17)	5024(12)	2492(9)	50(3)
C(9)	6345(18)	2894(13)	243(11)	56(3)
C(10)	3827(18)	3879(13)	608(10)	51(3)

[a] U_{eq} is defined as one third of the trace of the orthogonalised U_{ij} tensor.

ion. Assuming that there is some contribution from this structure in solution, the difference in chemical environments of the –CN groups may be attenuated. In order to examine this point more fully the solid-state ^{13}C-NMR spectrum of **31** was recorded. Fig. 1(a) shows the 75 MHz spectrum of **31** with pulse sequences for total suppression of spinning sidebands (TOSS) and Fig. 1(b) shows the combination of TOSS with dipolar dephasing (which suppresses non-quaternary carbon atoms). Interestingly, there is remarkably little variation in the chemical shifts of the Cp nuclei between DMSO solution in which the mean position is 123.17 ppm compared to the solid state (125.72 ppm) [28]. A similar phenomenon has been noted in the solid-state NMR

Table 3
Selected bond lengths (Å) and angles (°) for Tl[$C_5H_4C(CN)=C(CN)_2$]

N(1)–C(8)	1.13(2)	C(1)–C(6)	1.42(2)
N(2)–C(9)	1.11(2)	C(1)–C(5)	1.44(2)
N(3)–C(10)	1.14(2)	C(1)–C(2)	1.46(2)
C(2)–C(3)	1.36(2)	C(3)–C(4)	1.44(2)
C(4)–C(5)	1.38(2)	C(6)–C(7)	1.38(2)
C(6)–C(8)	1.50(2)	C(7)–C(9)	1.42(2)
C(7)–C10)	1.42(2)	Tl(1a)–C(1)	3.091(12)
Tl(1a)–C(2)	3.060(13)	Tl(1a)–C(3)	3.354(14)
Tl(1a)–C(4)	3.562(14)	Tl(1a)–C(5)	3.388(13)
Tl(1a)–N(1b)	3.242(13)	Tl(1a)–N(2d)	3.161(15)
Tl(1a)–N(3b)	3.160(13)	Tl(1a)–N(3c)	2.903(13)
C(6)–C(1)–C(5)	121.6(11)	C(6)–C(1)–C(10)	132.2(11)
C(5)–C(1)–C(2)	105.9(10)	C(3)–C(2)–C(1)	107.5(11)
C(2)–C(3)–C(4)	110.0(11)	C(5)–C(4)–C(3)	107.0(11)
C(4)–C(5)–C(1)	109.6(11)	C(7)–C(6)–C(1)	129.0(12)
C(7)–C(6)–C(8)	112.4(12)	C(1)–C(6)–C(8)	118.6(12)
C(6)–C(7)–C(9)	120.9(12)	C(6)–C(7)–C(10)	120.7(11)
C(9)–C(7)–C10)	118.4(11)	N(1)–C(8)–C(6)	175.5(14)
N(2)–C(9)–C(7)	173.0(20)	N(3)–C(10)–C(7)	175.9(13)

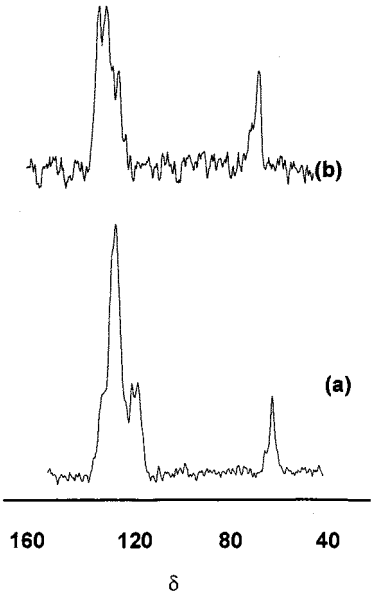

Fig. 1. The 75.5 MHz ^{13}C-solid-state NMR spectrum of Tl[$C_5H_4C(CN)=C(CN)_2$] (**31**) at 298 K; (a) normal spectrum; (b) with non-quaternary suppression.

spectrum of [Na(C_5H_5)TMEDA] (TMEDA = *N*, *N*, *N*′, *N*′-tetramethyl-1,2-ethanediamine) [29]. The vinylic carbons in **31** also show little variation in chemical shift between solid-state and solution spectra. The lower field signal in Fig. 1(b) shows three signals consistent with the differing environments of the nodal carbon, C(1) and the vinylic carbons. The upper field signal at 58.0 ppm is assigned to the CN carbon atoms. The appearance of this latter signal is supportive of a similar chemical environment for these carbons but the upfield shift of some 64 ppm compared to the solution spectrum reflects the relative dominance of substituent-metal bonding over Cp ring–metal bonding in this case. Compounds **10**, **12**–**13**, **15**–**18** and **20**–**23** in which an alkali metal is present and the ring substituents are the moderately accepting benozoyl, acetyl or formyl groups, show temperature dependent ^{13}C-NMR spectra. A typical example is given in Fig. 2 which shows the variation in spectral pattern for Cs(C_5H_4CHO) (**23**) over the range 30–100°C. At 100°C this compound shows one sharp signal for each of the atom pairs C(2), C(5) and C(3), C(4). Lowering the temperature results initially in line broadening and at 30°C three broad peaks are observed. Further reduction in temperature gives four peaks for C(2)–C(5). The persistently sharp signal due to C(1) strongly supports a fluxional process which involves rotation about the C(1)–C(6) bond. From the coalescence temperature (37 ± 2°C), the activation energy ($\Delta G^{\#}$) for this process was estimated as 57.3 ± 2 kJ mol^{-1}. In the series of compounds **10**–**24** there is a gradual increase in $\Delta G^{\#}$ in going from the benzoyl to the formyl ring substituent. For a given substituent, the variation in $\Delta G^{\#}$ follows the sequence

K > Li = Cs > Na > Tl. While the thallium(I) ion has a similar ionic radius [24] to potassium, its' greater softness and lower ionicity result in a preference for bonding to the ring carbon atoms rather than the heteroatom of the substituent. It is noteworthy that in the range of compounds **1**–**26** the chemical shifts of C(6) are consistently more deshielded for the thallium compounds. In a comparison of chemical shifts of $[M(C_5H_4C_6H_5F)]$ (M = Li, Na, K and Tl), Kordize [24] noted a similar deviation in chemical shift for the thallium compound and suggested that the presence of a 'sterochemically active' lone pair of electrons on the thallium(I) ion tends to result in repulsion of the solvent molecules.

In the present case, the trend in $\Delta G^{\#}$ values for the alkali metals reflects the balance between the cation solvation and its hardness. Thus, the smaller cation usually promotes formation of solvent-separated ion pairs because of more efficient solvation. However, it is also known that cations with a high charge density tend to distort the charge distribution in the neighbouring carbanion. For reasons which are not entirely clear, this phenomenon probably contributes to the maximum observed for the potassium salts. It is also apparent that the trends shown in Table 1 do stem from ionic aggregates which although solvated do not entirely prevent the cation from contributing to the nature of the bonding interaction. In this connection, Boche [25] found little change in the ^{13}C-NMR spectrum of $[Li(C_5H_4COMe)]$ when the solvent was altered from tetrahydrofuran (THF) to a 1:1 mixture of THF and hexamethylmethylphosphoric triamide (HMPA). In addition, the spectrum of this salt was temperature independent up to 55°C and gave signals consistent with population of isomer (**A**). Boche concluded that ion-pair effects were not decisive in determining the nature of the species in solution. However, in view of the results of Smid [4] for lithium fluorenide in THF solvent, it seems likely that these species are solvent-separated in both THF and HMPA. The difference in donor and acceptor characteristics of DMSO and HMPA [30] may then account for the difference in $\Delta G^{\#}$ values for $[Li(C_5H_4COMe)]$ in these solvents.

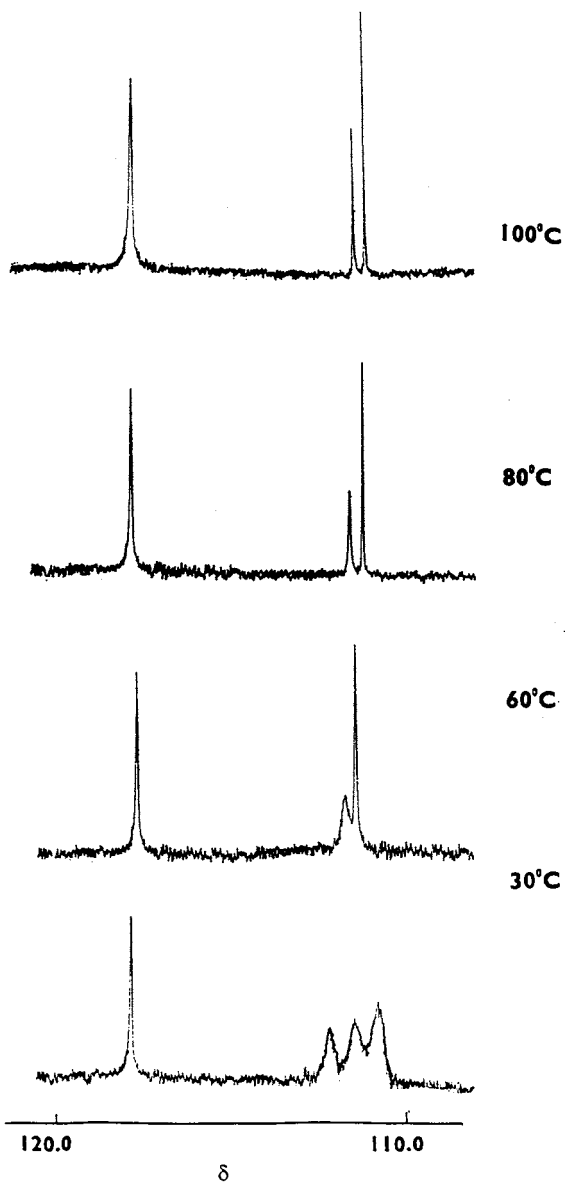

Fig. 2. Variable temperature ^{13}C-NMR spectra of $Cs(C_5H_4CHO)$ (**23**) in $(CD_3)_2SO$ at 62.89 MHz.

4.2. Discussion of the structure

The low temperature X-ray structure of **31** has previously been reported by Freeman et al. [31], the linear chain structure adopted being similar to that found for TlC_5H_5 [32]. Freeman et al. [31] noted, however, that crystallisation of **31** gave 'dark-red crystals of various morphological shapes'. In view of our NMR data for **31**, we decided to reinvestigate its structure crystallographically. We found the same unit cell for a variety of dark-red crystals of different morphologies, and this was in agreement with the results of the previous authors [31]. However, our analysis of the structure of **31** differs considerably from that previously reported [31] consisting of a complex 3D array whereby the thallium–cyclopentadienide chains are linked via thallium–nitrogen interactions. Fig. 3(a) shows the zig–zag nature of the chains and the linking of these chains is highlighted in Fig. 3(b). Thus, each metal is ligated somewhat asymmetrically to a single Cp ring, the distance from the midpoint of the ring centroids being 3.040 and 3.069 Å, with the individual contacts ranging from 3.060 to 3.562 Å, the shortest contact for both rings being to C(2). The co-ordination sphere is completed by four nitrogen atoms of the cyanide moieties. Two of these bind in a terminal fashion, (Tl–N(1) 3.242, Tl–N(2) 3.161 Å), while the third cyano nitrogen

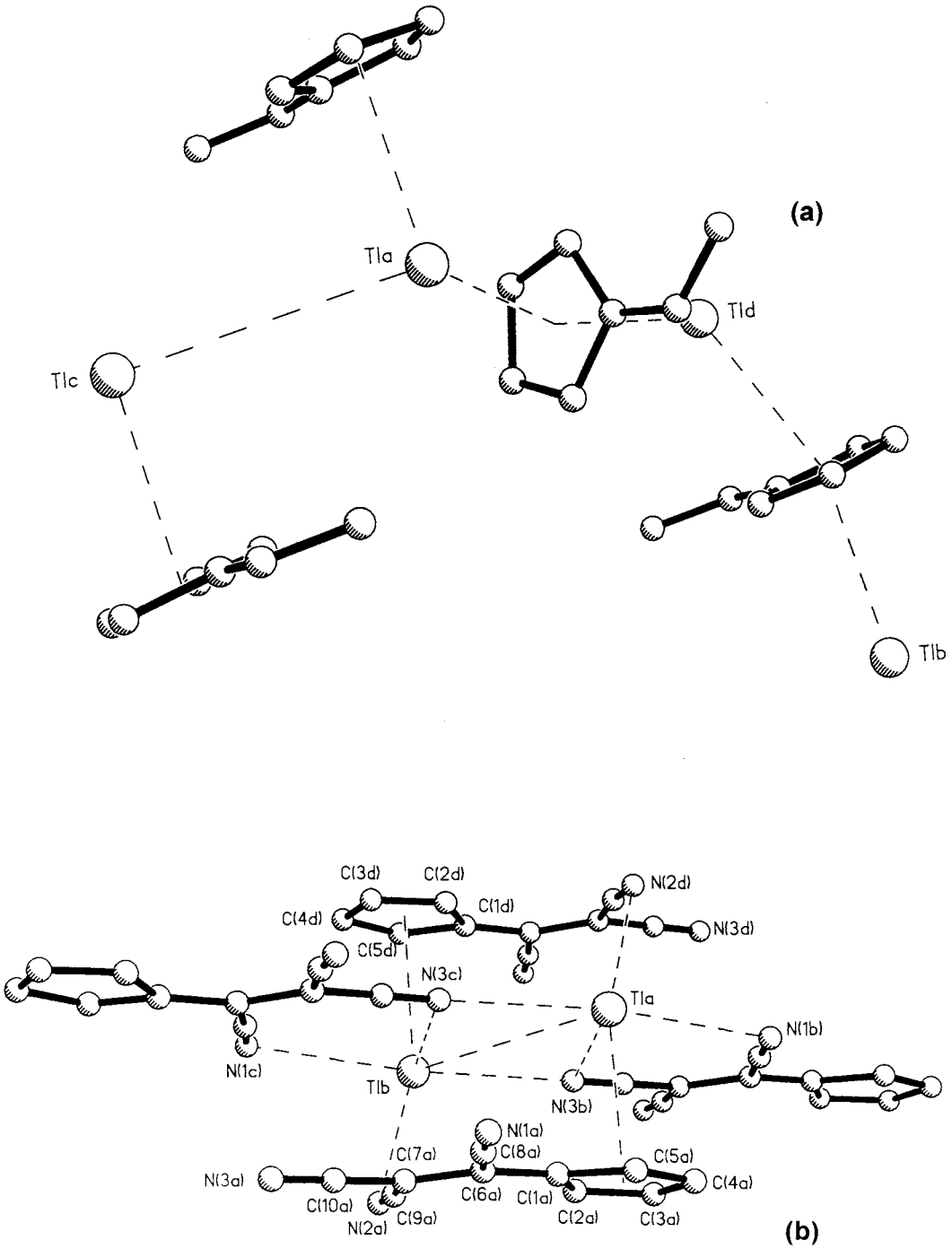

Fig. 3. The molecular structure of $Tl[C_5H_4C(CN)=C(CN)_2]$ (**31**) showing the numbering scheme; (a) detail of zig–zag chains; (b) linking of chains.

bridges the thallium–thallium vector asymmetrically (Tl(a)–N(3) 2.903, Tl(b)–N(3) 3.160 Å). Thus, each dithallium unit is linked to a total of four substituted cyclopentadienide rings, and all cyanide nitrogens are also bonded to the metal. To our knowledge, only one other complex has been crystallographically characterised in which a formally neutral nitrogen is bonded to thallium(I). Thus, in thallium(I) benzotriazolate [33], each metal atom has six co-ordinated nitrogen atoms at distances ranging from 2.725 to 3.326 Å. Very recently, the structure of thallium(I) bis(trimethylsilyl)amide has been shown [34] to contain short Tl–N contacts of 2.576 and 2.581 Å. Interestingly, the latter structure is also held together by in infinite chains by weak Tl–Tl contacts ranging from 3.650 to 3.933 Å. The structure of **31** represents an intermediate between the metal–ligand bonding observed in species such as $Tl(C_5Me_5)$ [35] and $Tl(C_5(CH_2Ph)_5)$ [36] in which there are, respec-

tively, zig–zag and linear polymeric chains of alternating Tl and C_5 units with metal–Cp bonding in which the co-ordination number of the metal is two and $Tl(C_5(CO_2Me)_5)$ in which the sole metal–ligand interaction involves the substituent carboxyl groups with a five–coordinate metal atom [37]. It is clear that this trend reflects the ionicity of the metal–ligand interaction. Although the latter bonding mode is also found for $K(C_5Cl_3(NO_2)_2)$ [38], in which the potassium ion is surrounded by six oxygen atoms of the nitro groups, the intermediate bonding situation has only been reported for the solvate $[Na(C_5H_4COMe)THF]$ [39]. In this case, the co-ordination sphere around each sodium atom consists of the oxygen atoms from two COMe ligands, an ion contact pair between the five Cp carbons and sodium, and an oxygen atom of the thf molecule. It is relevant to note that the degree of interaction involving metal and substituent heteroatoms in **31** exceeds that in $[Na(C_5H_4COMe)THF]$, this difference undoubtedly reflecting the greater importance of the fulvenoid conformer in the thallium salt. The structural features of the Cp ring in **31** do not vary appreciably between our analysis and the previous structure [31], both of which display a degree of fulvenoid character, e.g. the C(1)–C(6) distance of 1.42 (2) Å is comparable with the bond distances within the Cp ring and the C(6)–C(7) distance of 1.38(2) Å is somewhat longer than that found in tetracyanoethene, 1.317(5) Å [40]. Consistent with this are the bond distances C(7)–C(9), 1.42(2) and C(7)–C(10) 1.42(2) Å which are shorter than C(6)–C(8) 1.50(2) Å. That the bulk of this material consists of this unit cell was confirmed by a powder X-ray diffraction study, the results of which compare well with the simulated spectrum derived form the single-crystal data. It thus appears that the previous authors failed to make note of these potentially important thallium–nitrogen interactions. In order to explore more fully the role of the ring substituent and cation in contributing to the bonding in these systems a series of extended Hückel calculations were performed on a selection of compounds shown in Table 1.

4.3. Quantum chemical calculations

4.3.1. Method of calculation

We investigated the effect of two factors on the conformation of the ring substituent—the chemical natures of the metal atom M and of the substituent. In order to be able to 'tune' the atoms via a set of parameters, we selected a method based on extended Hückel theory (EHT) [41]. Both the orbital exponent ξ_i and the Coulomb term H_{ii} characterise the nature of AO i, but the results are more sensitive to the Coulomb term H_{ii} than to the orbital exponent ζ_i. For a comparison of the two series of investigations described—that of the metal and that of the substituent—we used the

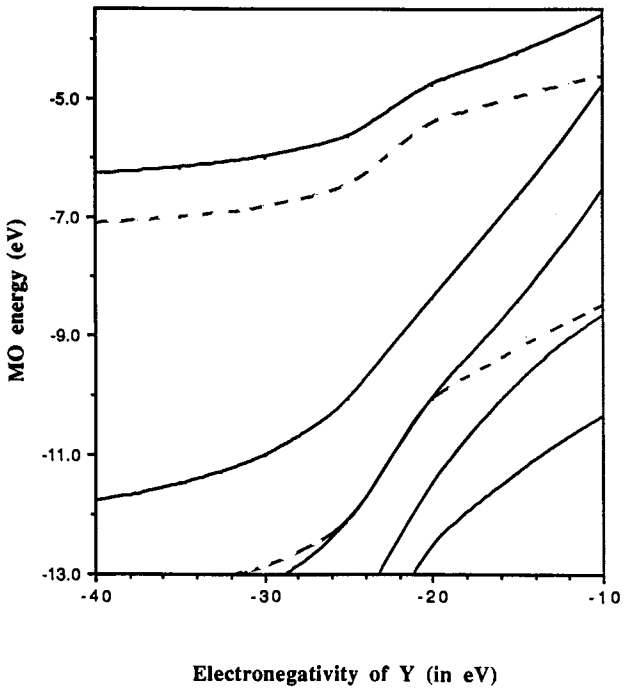

Fig. 4. The EHT-calculated energy levels of the π molecular orbitals in the $(C_5H_4CHY)^-$ anion as a function of the electronegativity of pseudo-atom Y. The continuous lines denote A′ (symmetric) MOs and broken lines those which are A″ (antisymmetric) in the C_s point group. The uppermost two MOs are vacant levels favourable for interaction with metal AOs.

procedure described in an earlier work [42] by fixing ζ at an average value and exploring the electronegativity ranges by 'tuning' the orbital energies H_{ii} alone. Since the ring substituents X in MC_5H_4X are all π–groups whose degrees of conjugation with Cp is central to the investigation, X was represented by H–C=Y, whose electron withdrawing power and conjugation with Cp is controlled through the Coulomb terms of the 2s and 2p AOs on the fictitious atom Y. The ionisation energies of the valence s AOs of neutral alkali metal atoms range from -5.4 eV for Li to -3.9 eV for Cs [43]. The negative shifts in these values that will accompany charge transfer from the valence shell will be accommodated by exploring the H_{ss} range. No attempt is made to include the non-alkali metal thallium. The Coulomb terms of the valence s and p AOs on Y are defined in a range of values based on H_{ii} energies of second and third row atoms. In accordance with the approximate factor of 2.0 relating the s and p Coulomb terms of light atoms [43], H_{pp} was taken to be one half of H_{ss}.

The complex features associated with solvation and bonding do not permit structures **A** and **B** to be compared by electronic energy calculations. We have used quantum chemical methods as a means of probing the energy barrier to torsion of the CHY substituent around the C(1)–C(6) bond for various characteristics of Y. As in our previous MO calculations on similar

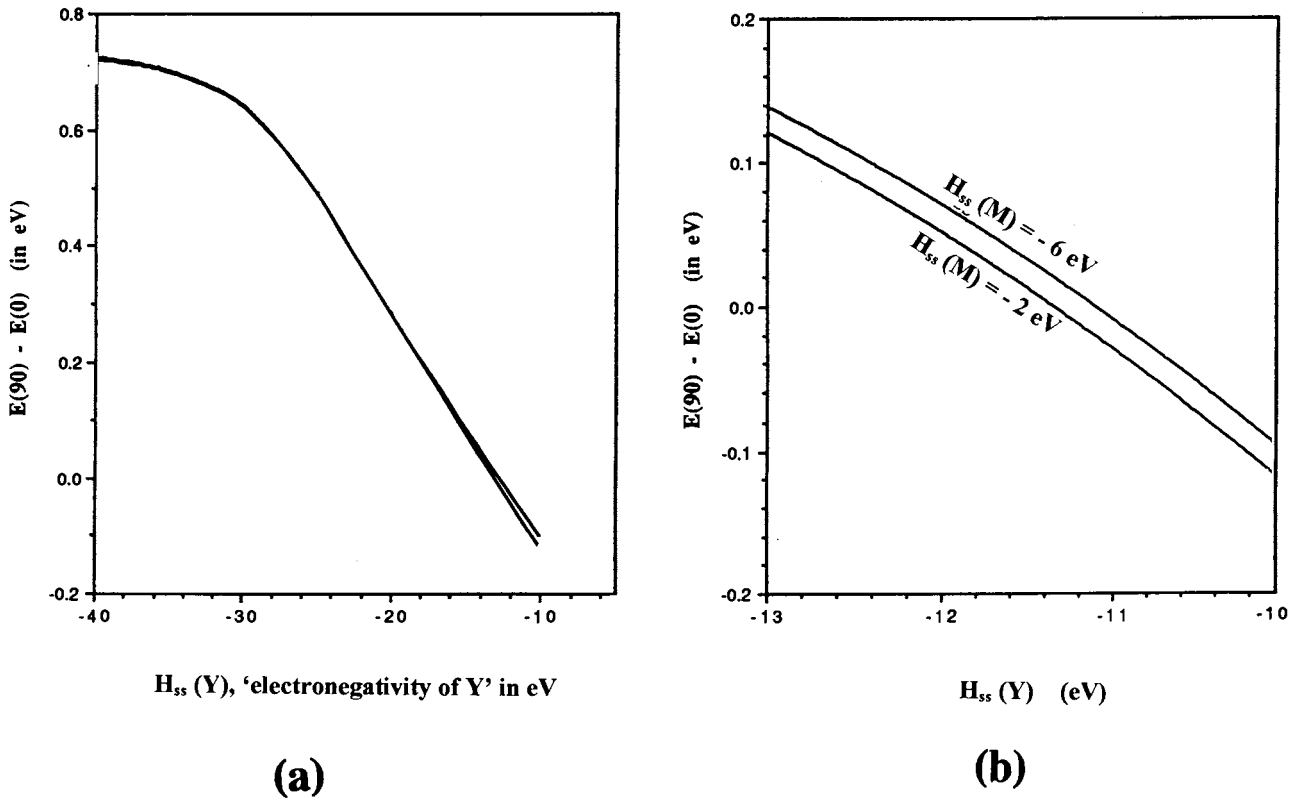

Fig. 5. The calculated energy barrier to torsion of the –CHY group; (a) the curves show the variation of ΔE_{tor} with the electronegativity H_{ii} of the pseudo-atom Y for a range of electropositive metal atoms M; (b) is a high resolution section of (a) to show the effect of varying H_{ii} of the M atoms. For an explanation of the electronegativity scale, see text.

systems [1], standard molecular bond lengths and angles were used to describe the geometry of the cyclopentadienyl ring. These were supplemented by the use of a constant perpendicular distance 2.0 Å between the metal atom and the ring centroid. The C=Y distance was taken as 1.36 Å and all the bond angles in CHY as 120°.

For each MCpCHY species selected, calculations were performed on two conformations—one with the CHY substituent coplanar ($\varphi = 0°$) and one with the substituent perpendicular ($\varphi = 90°$) to the Cp ring.

5. Results

5.1. Electronegativities

The effect of changing the electron withdrawing power of pseudo-atom Y is shown in Fig. 4, where ΔE_{tor}, the energy difference of the perpendicular over the planar conformer is plotted against H_{ss}, which may broadly be called the 'electronegativity' of Y (its accompanying term H_{pp} was also varied according to $H_{pp} = \frac{1}{2}H_{ss}$ in order to obtain the energies plotted in the figure). Since Y is a pseudo-atom, the identification of its parameters with real atoms or groups should be taken with caution. But using atomic orbital VSIEs to make a rough comparison, $H_{ss} = -30$ eV would correspond with an electronegativity between chlorine and oxygen, while that of -10 eV would describe iodine.

The figure shows an inclination to favour a planar, fulvenoid configuration (structure **A**) with $E(90°) \gg E(0°)$ for electron-withdrawing substituents with highly negative H_{ss} and H_{pp}. Those at the other end of the scale diminish the π-character of the C(1)–C(6) bond resulting in the condition $E(0°) > E(90°)$. This is in accord with Table 1, which shows an increasing torsional energy barrier with increasing electronegativity of X.

The high resolution ΔE plot included in Fig. 4(b) implies that increasing the electropositivity of the metal ion results in stabilisation of the cyclopentadienide relative to the fulvenoid conformation, reflecting the decreasing $\Delta G^{\#}$ values as M changes from Li to Cs. However, the effect is so slight that the bonding-type rôle played by the electropositivity of the metal atom in deciding between structures **A** and **B** is doubtful. A more decisive factor is probably that associated with the varying solvation effects of the cation M^+ which is neglected.

5.2. Metal–ring interaction

Quantum chemistry is not yet capable of reliably addressing those solvation considerations which decide the relative favourability of the **A** and **B** structures. However, the extended Hückel method can be used to describe the optimum conditions for the interaction between the metal atom and the Cp ring when the orbital parameters of M and Y are explored.

With the metal atom on the (almost) pentagonal axis of the Cp ring, then in the point-group C_s of MCpX, the ring's p-MOs may be classified as **A′** or A″ with respect to the plane containing the axis and the substituent X (or CHY). They interact with the metal atom's valence s and p AOs, respectively.

The most effective interactions will be those of the valence s and p AOs of M with those ring MOs of similar energy and of appropriate symmetry. We conducted iterative extended Hückel calculations [44] on the $(CpCHY)^-$ ligand in order to compare the MO energies with those of M on varying the electronegativity of Y. The results shown in Fig. 5 illustrate the dependence of the MO levels on the electronegativity, explored as before by varying H_{ss} and H_{pp}. Only the π-MOs are shown as the energy of the σ-MOs are not in the range of the metal atom's valence orbitals. Since the valence–AO H_{ss} and H_{pp} values of alkali metals are in the range -6 to -2 eV, the curves in Fig. 5 imply two facts. Firstly, the energy condition predicts that the Cp MOs which will interact most effectively with M will be the two highest ones, with symmetries A′ and A″, mixing with MO's valence s and p AOs, respectively. Secondly, as the monitoring parameter H_{ss} for atom Y becomes < -20 eV (which corresponds to a moderately electronegative atom), the energies of the ring MOs drop out of the -6 to -2 eV range of the alkali metals' valence AOs. Thus, the most efficient metal-to-ring interactions should be when the substituent has the least electron-withdrawing character. This is in agreement with both the conclusion in part (a) of this section and also the NMR observations in Table 1. As the substituent becomes more electronegative, the energies of the ring MOs are shifted out of the range appropriate for favourable interactions, destabilising the 'pentagonal axis' site of the M atom. Any association with CpX would then be through X. In fact, the stabilisation that we found for this position for strongly electron-withdrawing substituents X, defining structure **A**, can now be understood by the now strong negative charge on X resulting from its high electronegativity.

Acknowledgements

We thank Dr Ivan Parkin and Dr Elizabeth MacLean for assistance with the collection of X-ray powder diffraction data and Dr Abil Aliev for the solid-state NMR spectra.

References

[1] G. Hogarth, M. Arthurs, J.C. Bickerton, L. Daly, C. Piper, D. Ralfe, D.A. Morton-Blake, J. Organomet. Chem. 467 (1994) 145.
[2] J. Thiele, Chem. Ber. 23 (1900) 666.
[3] K. Hafner, G. Schulz, K. Wagner, Leibigs Ann. Chem. 678 (1964) 39.
[4] T.E. Hoghen-Esch, J. Smid, J. Am. Chem. Soc. 88 (1966) 307.
[5] M.L. Hays, T.P. Hanusa, Adv. Organomet. Chem. 40 (1996) 117.
[6] J.B. Grutzner, J.M. Lawlor, L.M. Jackman, J. Am. Chem. Soc. 94 (1972) 2306.
[7] R. Zerger, W. Rhine, G.D. Stucky, J. Am. Chem. Soc. 96 (1974) 5441.
[8] G. Boche, R. Eiben, W. Thiel, Angew. Chem. Int. Ed. Engl. 21 (1982) 688.
[9] A.L. van Geet, Anal. Chem. 42 (1970) 679.
[10] S.E. Kegley, A.R. Pinhas, Problems and Solutions in Organometallic Chemistry, Oxford University Press, London, 1987.
[11] H. Günther, Angew. Chem. Int. Ed. Engl. 11 (1972) 861.
[12] G.M. Whitesides, M. Witanoswki, J.D. Roberts, J. Am. Chem. Soc. 87 (1965) 2854.
[13] W.T. Dixon, J. Schaefer, M.D. Sefcik, E.O. Stejskai, R.A. McKay, J. Magn. Reson. 49 (1982) 341.
[14] Z. Song, O.N. Anzutkin, X. Feng, M.H. Levitt, Solid State Nucl. Magn. Reson. 2 (1993) 143.
[15] S. Opella, M.H. Fry, J. Am. Chem. Soc. 101 (1979) 5854.
[16] M. Arthurs, J.C. Bickerton, M. Kirkley, J. Palin, C. Piper, J. Organomet. Chem. 429 (1992) 245.
[17] M. Arthurs, M. Sloan, M.G.B. Drew, S.M. Nelson, J. Chem. Soc. Dalton. Trans. (1975) 1794.
[18] S.S. Jones, M.D. Rausch, T.E. Bitterwolf, J. Organomet. Chem. 450 (1993) 27.
[19] M. Arthurs, H.K. Al-Daffaee, J. Haslop, G. Kubal, M.D. Pearson, P. Thatcher, J. Chem. Soc. Dalton Trans. (1987) 2615.
[20] M. Arthurs, P. Gross, G. Kubal, L. Paniwnyk, E. Curzon, J. Organomet. Chem. 366 (1989) 223.
[21] R.C. Kerber, M.J. Chick, J. Org. Chem. 32 (1967) 1329.
[22] M.B. Freeman, L.G. Sneddon, Inorg. Chem. 19 (1980) 1125.
[23] M. Arthurs, S.M. Nelson, M.G.B. Drew, J. Chem. Soc. Dalton Trans. (1977) 779.
[24] A.A. Koridze, N.A. Ogorodnikova, P.V. Petrovsky, J. Organomet. Chem. 157 (1978) 145.
[25] G. Boche, R. Eiben, W. Thiel, Angew. Chem. (Suppl.) (1982) 1535.
[26] O.W. Webster, J. Am. Chem. Soc. 88 (1966).
[27] O.A. Gansow, A.R. Burke, Inorg. Nucl. Chem. Lett. 10 (1974) 291.
[28] R.K. Harris, Nuclear Magnetic Resonance Spectroscopy, Longman, Harlow, 1987.
[29] T. Pietras, P.K. Burket, Inorg. Chim. Acta 207 (1993) 253.
[30] V. Gutman, G. Resch, Lecture Notes on Solution Chemistry, World Scientific, Singapore, 1985.
[31] M.B. Freeman, L.G. Sneddon, J.C. Huffman, J. Am. Chem. Soc. 99 (1977) 5194.
[32] J.F. Berar, G. Calvarin, C. Pommier, D. Weigel, J. Appl. Crystallogr. 8 (1975) 366.
[33] J. Reedjik, G. Roelofsen, A.R. Siedle, A.L. Spek, Inorg. Chem. 18 (1975) 1947.

[34] K.W. Klinkhammer, S. Henkel, J. Organomet. Chem. 480 (1994) 167.
[35] H. Werner, H. Otto, H.J. Kraus, J. Organomet. Chem. 315 (1986) 57.
[36] H. Schumann, C. Janiak, M.A. Khan, J.J. Zuckermann, J. Organomet. Chem. 354 (1987) 7.
[37] M.I. Bruce, J.K. Walton, M.L. Williams, S.R. Hall, B.W. Skelton, A.H. White, J. Chem. Soc. Dalton Trans. (1982) 2209.
[38] Y. Otaka, F. Marumo, Y. Saito, Acta Crystallogr. B27 (1972) 1591.
[39] R.D. Rogers, J.L. Atwood, M.D. Rausch, D.W. Macomber, W.P. Hart, J. Organomet. Chem. 238 (1982) 79.
[40] D.N. Dhar, Chem. Rev. 67 (1967) 611.
[41] R. Hoffmann, J. Chem. Phys. 39 (1963) 1397.
[42] M. Arthurs, H. Karodia, M. Sedgwick, D.A. Morton-Blake, C.J. Cardin, H. Parge, J. Organomet. Chem. 291 (1985) 231.
[43] R.H. Summerville, R. Hoffmann, J. Am. Chem. Soc. 98 (1976) 7240.
[44] J. Howell, A. Rossi, D. Wallace, K. Araki, R. Hoffmann, Extended Hückel Program FORTICON 8, QCPE no. 344.